Tectonophysics 601 (2013) 177–191

Contents lists available at SciVerse ScienceDirect

Tectonophysics

journal homepage: www.elsevier.com/locate/tecto

Southern African perspectives on the long-term morpho-tectonic evolution of cratonic interiors

Alexandre Kounov [a,*], Giulio Viola [b,c], István Dunkl [d], Hartwig E. Frimmel [e,f]

[a] *Institute of Geology and Palaeontology, Basel University, 4056 Basel, Switzerland*
[b] *Geological Survey of Norway, 7491 Trondheim, Norway*
[c] *Department of Geology and Mineral Resources Engineering, Norwegian University of Science and Technology, 7491 Trondheim, Norway*
[d] *Sedimentology and Environmental Geology, Geoscience Center, University of Göttingen, 37077 Göttingen, Germany*
[e] *Institute of Geography and Geology, University of Würzburg, 97074 Würzburg, Germany*
[f] *Department of Geological Sciences, University of Cape Town, Rondebosch 7700, South Africa*

ARTICLE INFO

Article history:
Received 4 December 2012
Received in revised form 2 May 2013
Accepted 11 May 2013
Available online 23 May 2013

Keywords:
Fish River Canyon
Orange River
Fission-track
(U–Th–[Sm])/He
Denudation
Paleorelief

ABSTRACT

We propose a refined conceptual model for the Paleo- and Mesozoic morpho-tectonic evolution of the southern African cratonic interior. Constraints are derived from new zircon and apatite fission-track and (U–Th–[Sm])/He dates (ZFT, AFT, ZHe and AHe) of rocks from the Augrabies Falls and Fish River Canyon regions in South Africa and southern Namibia, respectively. The combined ZFT and ZHe thermochronological results suggest a smooth and simple tectonic evolution, wherein the study area cooled monotonically as one coherent block from the Early Silurian to the Mid Triassic in response to very low denudation rates of less than 5 m/myr. Some of the new zircon ages may indicate a discrete and short-lived period of enhanced cooling interrupting this monotonic cooling during the Mid Devonian–Early Carboniferous. We tentatively correlate this episode to the events that caused the regional hiatus that separates the Cape Supergroup from the overlying Karoo Supergroup.

Apatite fission-track and (U–Th–[Sm])/He data joint modeling reveals a period of accelerated regional cooling through 120 to 40 °C between 100 and 65 Ma ago. We interpret the latter as most probably due to regional uplift in combination with high river gradients and enhanced erosion rates in the Orange and Fish River basins, which, during the Cretaceous, were probably part of the greater Kalahari River catchment area. Based on the apatite results, a denudation rate of ca. 25 m/myr was calculated for the Late Cretaceous. At that time the area was probably characterized by an elevated average altitude and low relief, as indicated by the AFT and AHe age patterns.

1. Introduction

Reconstructing the morpho-tectonic evolution of old cratons is a challenging task due to the fact that their sedimentary sequences and other geological records that postdate the consolidation of the cratons are in most areas almost completely absent due to erosion or are only very marginally preserved. Among the world cratonic areas the southern African interior is atypical due to its present-day elevated topography, at odds with the fact that it is surrounded exclusively by continental passive margins (Fig. 1; see review by de Wit, 2007). Southern African passive margins are defined by a gentle, seaward-inclined low coastal plain that is separated from an elevated inland plateau by a seaward facing escarpment (the "Great Escarpment" of King, 1953, Fig. 1). Research during the last twenty years has improved significantly our understanding of the Mesozoic and Cenozoic thermal and tectonic evolution of those margins (e.g. Brown et al., 2000, 2002; Cockburn et al., 2000; Fleming et al., 1999; Flowers and Schoene, 2010; Kounov et al., 2007, 2008, 2009; Raab et al., 2002; Tinker et al., 2008). Much of the early post-Pan-African thermal and tectonic evolution of the South African interior remains poorly explored and understood. Most attempts to reconstruct its Paleozoic and Early Mesozoic geological evolution are based on morphological (e.g. Andreoli et al., 1996; Burke, 1996; Burke and Gunnell, 2008; King, 1953; Moore, 1999; Partridge, 1998; Partridge and Maud, 1987; Roberts and White, 2010) and/or structural considerations (Basson and Viola, 2003, 2004; Viola et al., 2012). A common problem with the morphological and the structural approach, though, is the paucity of reliable geochronological control on the correlative features used to elaborate regional models and of robust constraints on the regional rates of denudation. Only a few quantitative geochronological constraints exist as of today (e.g. Brown et al., 1990, 2000; Kounov et al., 2009; Tinker et al., 2008), which in turn hampers a thorough understanding of the southern African cratonic morpho-tectonic evolution.

In this study we propose a new conceptual model of the geological evolution of the southern African interior based on new geochronological investigations of the Augrabies Falls and Fish River Canyon regions (Fig. 2). We studied these areas because they permit access to a significant elevation difference between deeply entrenched riverbeds and the top of the surrounding interfluves (Fig. 2). In areas with little tectonic

* Corresponding author. Tel.: +41 612670484.
E-mail address: a.kounov@unibas.ch (A. Kounov).

0040-1951/$ – see front matter © 2013 Elsevier B.V. All rights reserved.
http://dx.doi.org/10.1016/j.tecto.2013.05.009

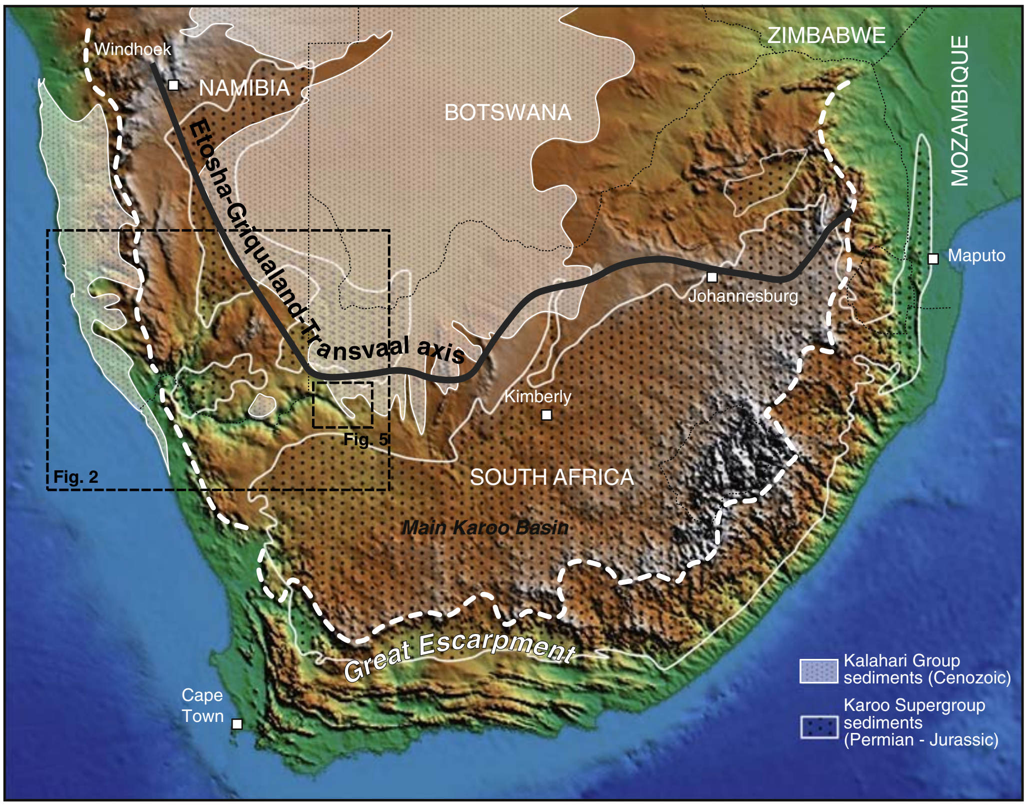

Fig. 1. Colored relief map of southern Africa. The thick, dark gray line represents the Etosha–Griqualand–Transvaal flexural axis and the white dashed line the present-day position of the Great Escarpment.

activity, such as cratonic interiors, low-temperature age–altitude plots provide a reliable approach to the study of slow processes of denudation. In addition, the concomitant application of multiple low-temperature thermochronological methods (each characterized by a different thermal sensitivity) makes it possible to decipher the geological evolution of large areas for a significant range of temperature and time intervals.

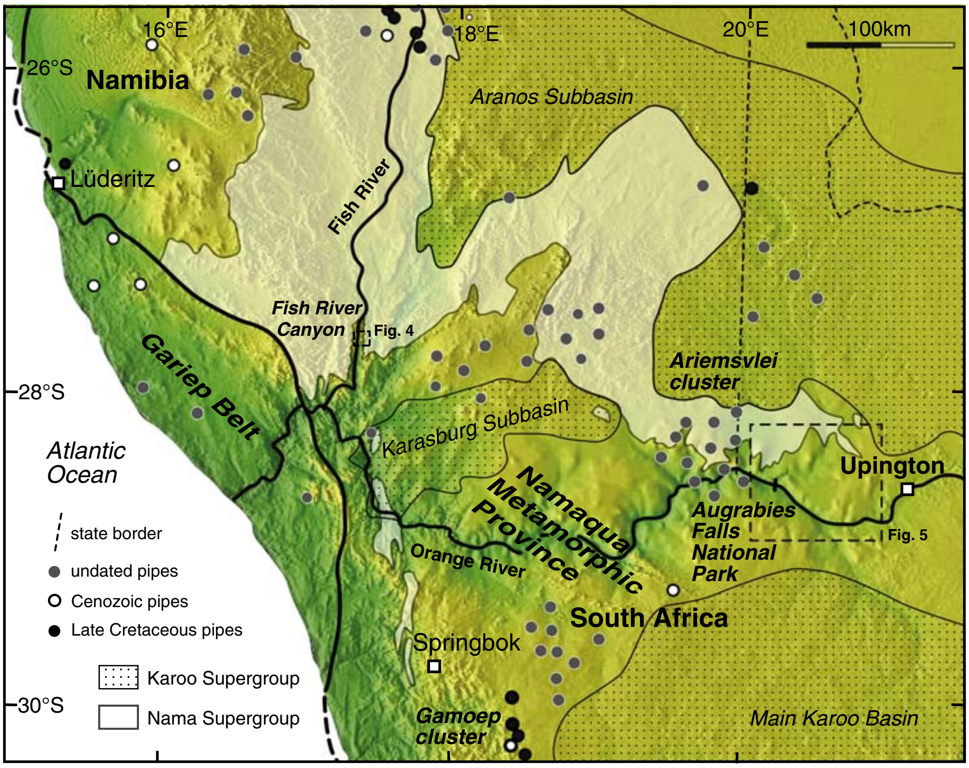

Fig. 2. Colored relief map of southern Namibia and northern South Africa, with the lower courses of the Fish and Orange Rivers.

To reconstruct the thermal evolution of the southern African interior from the Paleozoic to the end of the Cretaceous, we used fission-track and (U–Th–[Sm])/He analysis on zircon and apatite (ZFT and AFT, and ZHe and AHe, respectively).

2. Geological and morphological setting of the study area

The geology of the Augrabies Falls and Fish River Canyon areas is dominated by gneisses of the Mesoproterozoic Namaqualand Metamorphic Province (NMP, Fig. 2; e.g. Cornell et al., 2006). Exhumed during the Early Neoproterozoic (between 1000 and 800 Ma), the NMP metamorphic basement is overlain by the sedimentary Upper Ediacaran to Lower Cambrian Nama Group (Gresse et al., 2006; Fig. 2). Near the Late Precambrian Pan-African Gariepian orogenic front in the west, the Nama Group rocks were deformed and metamorphosed at very low grade, together with their NMP basement, in the course of a late Pan-African tectonic pulse at around 535 Ma (Grotzinger et al., 1995) and subsequent brittle/ductile deformation with corresponding Ar–Ar ages as young as 491 Ma (Frimmel and Frank, 1998). In the study area the Nama Group is represented by a thin and undeformed sequence of predominantly siliciclastic sedimentary rocks (Fig. 2, Gresse et al., 2006). It has been suggested that the NMP entered the brittle realm already in the Early Neoproterozoic (see Viola et al., 2012) and that several brittle deformational phases were accommodated since that time (e.g. Cornell et al., 2006; Eglington, 2006; Frimmel and Frank, 1998; Viola et al., 2012). From the Late Carboniferous to the Early Jurassic, the Karoo Supergroup, which consists of a several kilometer thick succession of siliciclastic sedimentary rocks, was deposited over large parts of Southern Africa (Fig. 1). Sedimentation took place in a large foreland basin, probably formed in response to the orogenic load of the Cape Fold Belt to the south (Thamm and Johnson, 2006). This large foreland basin was subsequently dismembered into several smaller sub-basins and the large Main Karoo Basin (Fig. 1, Johnson et al., 2006). Examples of the smaller sub-basins in the larger study area are the Aranos Subbasin, containing Upper Carboniferous–Lower Permian Dwyka Group continental sediments, and the Karasburg Subbasin, just south of the Fish River Canyon, with sediments of the Dwyka and Ecca groups (Fig. 2). During the evolution of these Late Carboniferous–Permian basins the studied areas formed part of the so-called Cargonian Highland (Veevers et al., 1994).

The ca. 170–150 Ma break-up of Gondwana (e.g. Hawkesworth et al., 1999) started with the separation of West Gondwana (Africa and South America) from East Gondwana (Australia, Antarctica, India and New Zealand), following the extrusion of the voluminous and extensive continental flood basalts of the Drakensberg Group (184–174 Ma; Jourdan et al., 2007), and the emplacement of numerous dolerite sills (Karoo magmatic event). The break-up of West Gondwana between 144 and 125 Ma started with rifting, accompanied along the continental margins by the emplacement of syenite and granite plutons as well as dolerite dykes (e.g. Eales et al., 1984; Reid and Rex, 1994; Trumbull et al., 2007). The opening of the South Atlantic was characterized by the northward propagation of the spreading center over a period of around 40 myr, with sea-floor spreading beginning at about 134 Ma (Eagles, 2007; Rabinovich and LaBrecque, 1979). Concomitant with the early drift phase, numerous mafic alkaline intrusions, including kimberlites and related rocks, were emplaced across Southern Africa. Two distinct peaks in the timing of kimberlite emplacement were reported at 145–115 and 95–80 Ma, corresponding to Kimberlite Group II and I, respectively (e.g. Basson and Viola, 2004; Smith et al., 1985). Subsequently, two further clusters of kimberlitic plugs formed in Namaqualand, the older (~77–54 Ma) is referred to as the Gamoep cluster (Fig. 2) and the younger (56–38 Ma) as the Bitterfontein cluster (Phillips et al., 2000). West of the Augrabies area crops out the supposedly Late Cretaceous kimberlitic pipes of the Ariemsvlei cluster (Fig. 2, Moore et al., 2008; Skinner and Truswell, 2006).

No significant regional tectonic events since the Early Cambrian have been noted in the area. Recent studies on the low-temperature thermal history indicate a well constrained Mid Cretaceous (115–80 Ma) phase of accelerated denudation, related to continental uplift, affecting not only the Southern African margin but also its most proximal interior (e.g., Brown et al., 2000; Kounov et al., 2009; Tinker et al., 2008).

2.1. Fish River Canyon

The Fish River Canyon forms a 160 to 550 m deep gorge cut through flat-lying Nama sedimentary rocks and underlying gneisses of the NMP, with a nonconformable contact readily seen in the canyon walls (Fig. 3a). Along its upper 450 km (of a total length of approximately 650 km) the river flows within a low-gradient broad valley. Downstream, the gradient increases, causing the Fish River to incise dramatically. The river must have initially flowed slowly over a flat land surface where it could meander freely as shown by its numerous bends, but continental uplift caused base level drop and the deep incision of the river into this surface to its present day level.

Numerous faults and several graben structures parallel to present day river course are shown on existing geological maps (e.g. Mvondo et al., 2011), and are readily seen in the field. Several of these fault zones are presently exploited by hot groundwater and associated hot springs. The age of these faults is not well constrained but they certainly postdate the Jurassic Karoo sedimentary rocks as they cut through them. Mvondo et al. (2011) report Eocene to Pleistocene ages for some of these structures. One such fault, with a clear reverse sense of movement, affects the vertical section sampled within the Fish River Canyon (Figs. 3b and 4).

Samples for apatite and zircon fission track dating and (U–Th–[Sm])/He analysis were collected along a profile from the lower to the upper reaches of the Fish River Canyon (Fig. 4).

2.2. Augrabies area

The study area comprises the Augrabies Falls National Park and neighboring areas (referred to as "Augrabies area" from hereon, Fig. 5). The Augrabies Falls are located ca. 100 km west of Upington (Fig. 2) and represent the major knickpoint of the Orange River that forms the regional base level for the upper ~650 000 km^2 of the Orange Basin. As the river approaches the falls, it divides into numerous channels before cascading down a 56 m high waterfall system. The river continues then along an 18 km long and about 240 m deep gorge, cut into the gneisses of the NMP (Fig. 3c). There are no significant ductile structures that deformed the Mesoproterozoic basement, thus excluding substantial tectonic activity over the past 1000 myr.

In the Augrabies area, samples for apatite and zircon fission track and (U–Th–[Sm])/He analysis were collected along traverses across the Orange and Molopo rivers (Fig. 5). Samples were also collected along one vertical section in the Orange River gorge (Figs. 3 and 5).

3. Low-temperature thermochronological analysis

3.1. Fission-track analysis

The fission-track (FT) analytical procedure and methodology are described in Appendix A. The geographical location of the samples and the results are presented in Figs. 4, 5 and 6, and Tables 1 and 2.

3.1.1. Zircon fission-track data

From the Augrabies area only three zircon samples could be analyzed. A granitic dyke transposed parallel to the regional high-grade planar fabric of the NMP gneisses (sample AG09) yielded a zircon FT age of 367 ± 23 Ma (Table 1, Fig. 6). The other two samples AG01 and AG06 yielded zircon FT ages of 439 ± 49 and 420 ± 50 Ma, respectively. Sample AG01 is a Proterozoic quartzite, whereas AG06 is

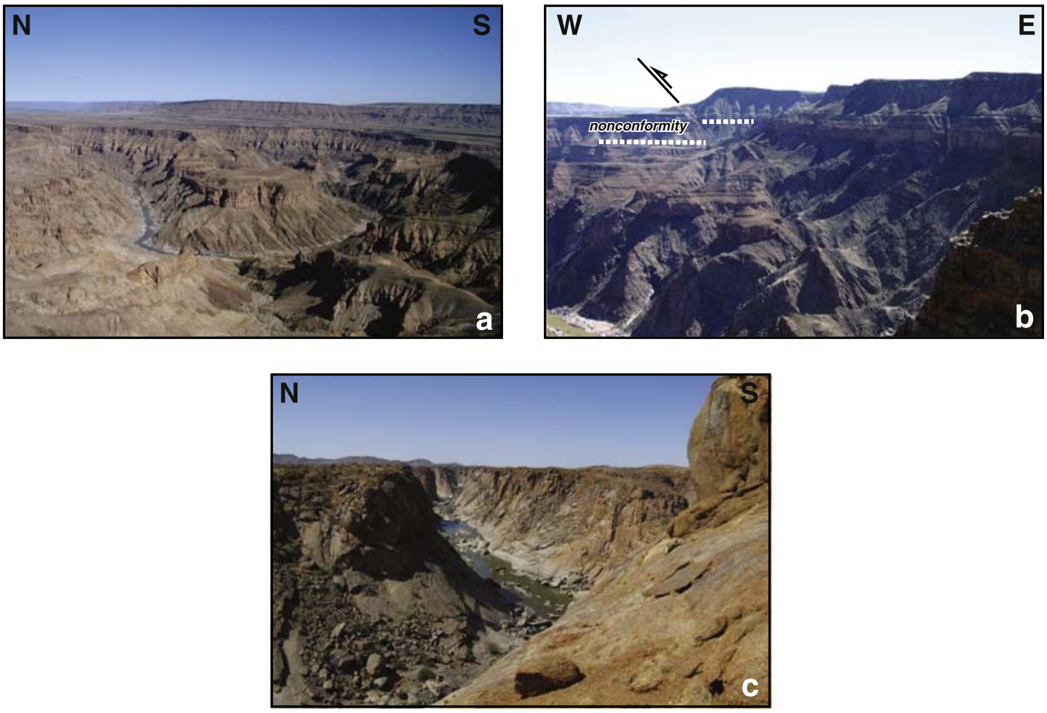

Fig. 3. (a) Fish River Canyon viewed from the west. (b) View to the north of a discrete brittle reverse fault. (c) Orange River Gorge at the Augrabies Falls National Park.

a granitic pebble from the base of the Nama Supergroup basal conglomerate (Fig. 6).

3.1.2. Apatite fission-track data

3.1.2.1. Fish River Canyon. Five samples were analyzed from the vertical profile within the Fish River Canyon. The three samples from the lower part of the canyon yielded statistically identical ages between 81 ± 10 Ma and 83 ± 17 Ma, the sample from within the fault zone core gave an age of 70 ± 11 Ma (FRC06) and that from the hanging wall an age of 67 ± 26 Ma (FRC09; Table 2, Fig. 4). In only one sample (FRC03) from this area was it possible to measure enough horizontal confined tracks for meaningful modeling of the data (Fig. 7).

3.1.2.2. Augrabies area. Ten apatite samples were dated from different altitudes along a section extending from 437 to 930 m asl (Table 1, Fig. 5). Four of them were collected from within the Orange River gorge (samples AG08 to AG11). All samples are high-grade gneisses of the NMP except sample AG06, the granitic pebble from the Nama Group sediments mentioned above (Fig. 5). Ages show a relatively narrow distribution from 93 ± 10 Ma to 83 ± 7 Ma, with a strong positive correlation between age and altitude (Fig. 8). In five samples sufficient

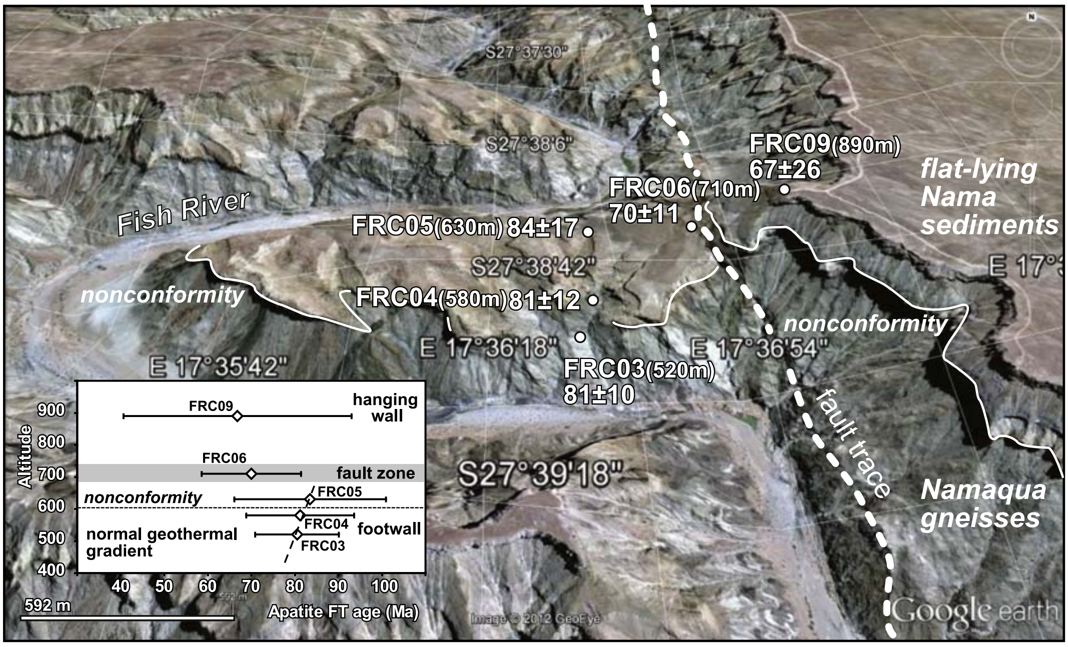

Fig. 4. High-resolution Google Earth image of the Fish River Canyon. Inset: age–altitude plot of the AFT samples.

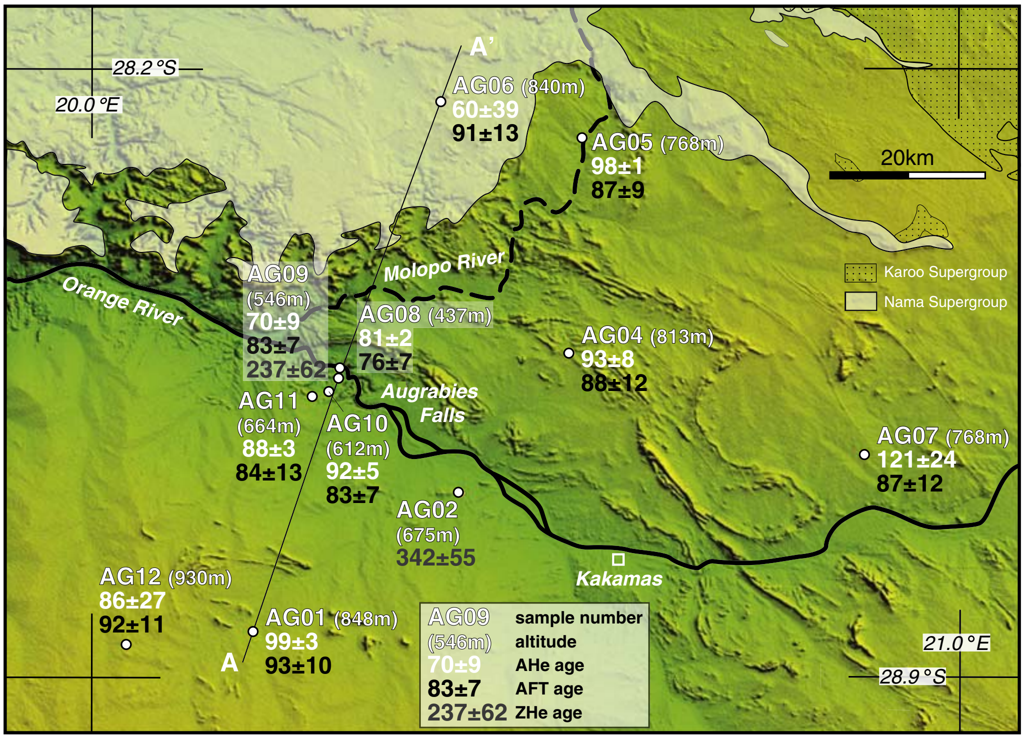

Fig. 5. Colored relief map of the Augrabies area with the position of the analyzed samples and the obtained geochronological results. A–A': trace of the section shown in Fig. 6.

numbers of horizontal confined track lengths were measured for reliable modeling of their thermal evolution (Fig. 6).

3.2. (U–Th–[Sm])/He analysis

The (U–Th–[Sm])/He analytical procedure and methodology are described in Appendix B. The geographical location of the samples and the results are presented in Fig. 5 and Table 3.

3.2.1. Zircon He data

Zircon grains from two samples were dated from the Augrabies area with good reproducibility (Table 3). In sample AG02 (342 ± 55 Ma, Fig. 5) two replicates reproduce within 2σ and were used for our final mean age calculation (Table 3). For sample AG09 (237 ± 62 Ma, Fig. 5) two out of three replicates reproduce within 2σ error.

3.2.2. Apatite He data

Samples from the Augrabies area dated by apatite fission-track were also dated by AHe (Table 3, Fig. 5). In general, the AHe data reproduce well. Only two samples yielded ages younger than the AFT ages: samples AG09 (70 ± 9 Ma) and AG12 (86 ± 27 Ma), although all analyzed samples have AFT and AHe ages overlapping within their 2σ errors (Fig. 8). The only exception are samples AG06 (60 ± 39 Ma) and AG07 (121 ± 24 Ma), which, although overlapping within the 2σ interval and although being characterized by a larger error than the other samples, gave nominally distinct AHe and AFT ages.

3.3. Modeling of the thermal history

Fission tracks in apatite form continuously through time, with an initial mean length of ~16.3 μm (Gleadow et al., 1986). Upon heating, tracks gradually anneal and shorten to a length that depends on the

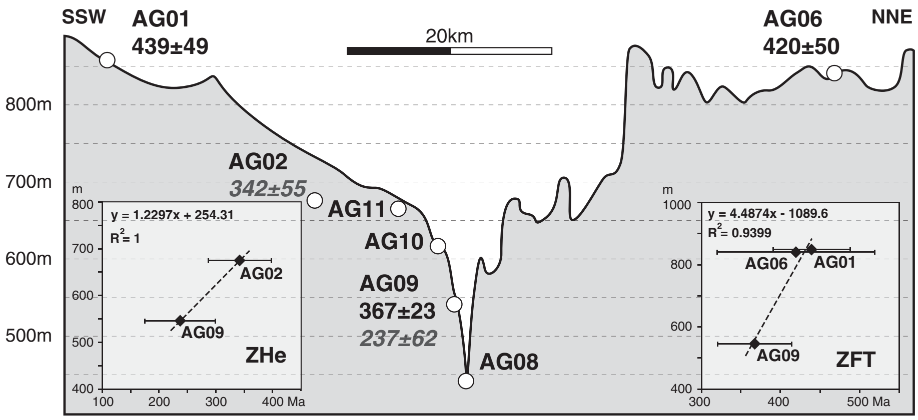

Fig. 6. Schematic cross-section across the Augrabies area and age–altitude plots for the ZHe and ZFT results. Regular font: ZFT ages; Gray italic font: ZHe ages.

Table 1
Fission track results from the Augrabies Falls area.

Sample number	Latitude/ longitude	Alt. m	Lithology	Strat. division	Min. anal.	Num. gr.	ρd(Nd) $\times 10^6$ cm^{-2}	ρs (Ns) $\times 10^6$ cm^{-2}	ρi (Ni) $\times 10^6$ cm^{-2}	P(χ^2) (%)	U. conc. (ppm)	Central age (±2σ)Ma	MTL(±1σ) μm	Std. dev.(N) μm	Dpar μm
AG01	S28.8476/ E20.18527	848	Quartzite	NMC	AP	23	1.350 (7633)	0.597 (658)	1.430 (1576)	99	13 ± 5	**93.0 ± 9.8**	13.59 ± 0.13	1.29 (100)	1.9
					ZR	16	0.421 (3434)	6.267 (1617)	0.3537 (91)	97	41 ± 30	**439.4 ± 48.7**			
AG04	S28.52775/ E20.55217	813	Gneiss	NMC	AP	21	1.312 (7633)	0.523 (339)	1.293 (838)	100	13 ± 6	**87.6 ± 12**			1.9
AG05	S28.27875/ E20.56771	768	Granitic dyke	NMC	AP	20	1.299 (7633)	1.285 (757)	3.156 (1859)	89	28 ± 8	**87.3 ± 8.6**			1.9
AG06	S28.23809/ E20.40268	840	Granite clast	Nama Group	AP	20	1.292 (7633)	0.308 (301)	0.720 (703)	100	8 ± 6	**91.3 ± 13.4**			2.7
					ZR	11	0.419 (3434)	19.82 (1342)	1.167 (79)	99	90 ± 16	**419.5 ± 99.6**			
AG07	S28.64418/ E20.88997	802	Granodiorite	NMC	AP	28	1.273 (7633)	0.522 (378)	1.259 (911)	99	13 ± 12	**87.2 ± 11.6**	13.36 ± 0.10	0.94 (84)	1.9
AG08	S28.5465/ E20.28621	437	Granite gneiss	NMC	AP	20	1.254 (7633)	1.369 (1068)	3.732 (2911)	100	35 ± 9	**76.0 ± 6.6**	13.47 ± 0.11	1.08 (101)	2
AG09	S28.55488/ E20.28423	546	Granitic dyke	NMC	AP	20	1.241 (7633)	1.735 (984)	4.303 (2440)	97	42 ± 10	**82.7 ± 7.4**	13.65 ± 0.12	1.24 (100)	2.1
					ZR	27	0.423 (3434)	21.54 (4677)	1.464 (318)	100	113 ± 29	**367.4 ± 46.8**			
AG10	S28.57133/ E20.27383	612	Kfs porph. granite	NMC	AP	20	1.235 (7633)	1.696 (975)	4.186 (2407)	97	39 ± 9	**82.6 ± 7.4**	13.46 ± 0.12	1.17 (101)	2
AG11	S28.57802/ E20.25365	664	Para-gneiss	NMC	AP	21	1.216 (7633)	0.283 (267)	0.680 (642)	99	7 ± 3.4	**83.5 ± 12.8**			3.6
AG12	S28.86349/ E20.03967	930	Granite	NMC	AP	23	1.203 (7633)	0.588 (506)	1.274 (1097)	90	14 ± 5	**91.6 ± 10.8**			2.4

All ages are central ages (Galbraith, 1981). $\lambda D = 1.55125 \times 10^{-10}$. A geometry factor of 0.5 was used. Zeta = 332 ± 7 for CN5/apatite and 122 ± 2 for CN1/zircon. Irradiations were performed at the OSU facility, Oregon State University Radiation Center, USA. P(χ^2) is the probability of obtaining χ^2 values for ν degrees of freedom where ν = number of crystals − 1. ρd, ρs and ρi represent the standard, sample spontaneous and induced track densities respectively. MTL – mean track length. Std. dev. – standard deviation. Dpar — mean track pit length. All numbers in brackets are numbers of measurements. NMC – Namaqua Metamorphic Complex.

Table 2
Apatite fission track results from the Fish River Canyon.

Sample number	Grid references	Alt. m	Lithology	Strat. division	Num. gr.	ρd(Nd) $\times 10^6$ cm^{-2}	ρs(Ns) $\times 10^6$ cm^{-2}	ρi(Ni) $\times 10^6$ cm^{-2}	P(χ^2) (%)	U. conc. (ppm)	Central age (±2σ)Ma	MTL (±1σ) μm	Std. Dev. (N) μm	Dpar μm
FRC09	S27°38.601′/ E17°37.002′	890	Sandstone	NG	4	1.248(5824)	0.660(35)	2.038(108)	94	25 ± 20	**66.8 ± 26.2**			2.47
FRC06	S27°38.620′/ E17°36.771′	710	Sandstone	NG	14	1.229(5824)	0.795(221)	2.306(641)	94	24 ± 10	**70.0 ± 11.4**			2.38
FRC05	S27°38.607′/ E17°36.535′	630	Sandstone	NG	7	1.201(5824)	1.007(139)	2.391(330)	94	25 ± 16	**83.5 ± 17.4**			2.51
FRC04	S27°38.770′/ E17°36.515′	580	Gneiss	NMC	15	1.260(5824)	1.451(283)	3.718(725)	36	35 ± 14	**81.2 ± 12.4**			2.1
FRC03	S27°38.828″/ E17°36.498″	520	Gneiss	NMC	20	1.260(5824)	0.404(471)	1.044(1217)	96	10 ± 3	**80.5 ± 9.6**	13.80 ± 0.11	0.97 (83)	2.45

All ages are central ages (Galbraith, 1981). λD = 1.55125 × 10^{-10}. A geometry factor of 0.5 was used. Zeta = 332 ± 7 for CN5. Irradiations were performed at the OSU facility, Oregon State University Radiation Center, USA. P(χ^2) is the probability of obtaining χ^2 values for ν degrees of freedom where ν = number of crystals − 1. ρd, ρs and ρi represent the standard, sample spontaneous and induced track densities respectively. MTL — mean track length. Std. Dev. — standard deviation. Dpar — mean track pit length. All numbers in brackets are numbers of measurements. NG — Nama Group sediments. NMC — Namaqua Metamorphic Complex.

integrated effect of the thermal overprint (duration and temperature). For example, tracks become completely annealed at a temperature of 110–120 °C for a period of 10^5–10^6 years (Gleadow and Duddy, 1981). Annealing characteristics make it possible to generate time-temperature paths by inverse modeling (e.g. Gallagher and Sambridge, 1994; Ketcham, 2005; Ketcham et al., 2000). Low-temperature thermal histories for our samples were modeled using the software HeFTy (Ketcham et al., 2000). Fission-track age, track-length distribution and etch-pit diameters (Dpar), in combination with user-defined time–temperature (t–T) boxes, as well as (U–Th–[Sm])/He data, served as our input parameters. An inverse Monte Carlo algorithm with a multi-kinetic annealing model (Ketcham et al., 2007) was used to generate time–temperature paths. The algorithm generated a large number of time–temperature paths, which were tested against the input data, that is, the t–T paths are forced to pass through user-defined time–temperature boxes. The fit between measured and modeled data was evaluated statistically and quantified by the so-called "goodness of fit" value (GOF). A "good" result corresponds to GOF values > 0.5, whereas a value between 0.5 and 0.05 is considered to reflect an "acceptable" fit between modeled and measured data. The software operates with the diffusion kinetics parameters of the Durango apatite (Farley, 2000). As suggested by the uniform distribution of track densities within individual crystals, we assume a homogenous distribution of U and Th in the dated apatite grains. One exception is sample AG07, characterized by a heterogeneous distribution of fission tracks and thus of U content. As a consequence the sample was modeled by using only the fission-track data. The heterogeneous distribution of U and Th in the crystals is probably also the reason for the anomalously high (U–Th–[Sm])/He age of this sample compared to the fission-track age (Meesters and Dunai, 2002). Another sample where the modeling is based only on fission-track data is FRC03; this is due to the impossibility of obtaining (U–Th–[Sm])/He ages for that sample.

We modeled the thermal history five samples from the Augrabies area and one from the Fish River Canyon (Fig. 7). These are the samples with more than 80 confined horizontal tracks, which enables one to conduct statistically robust thermal modeling (Tables 1 and 2). All modeling results are illustrated by 50 "good" (GOF > 0.5) individual cooling paths (Fig. 7, gray lines) as well as by the "best fit" (thin dashed black lines in Fig. 7) and the "weighted mean" (thick black lines in Fig. 7) paths obtained for each sample. Time–temperature boxes were defined for the three time intervals 200–120 Ma, 120–60 Ma and 60–0 Ma (Fig. 7). The time dimension of the first box overlaps with the youngest obtained zircon He age, which suggests that at some point during that time interval the studied rocks were at a temperature higher than 120 °C. The second box overlaps with a well-established period of regional accelerated cooling in Southern Africa, as reported by numerous previous studies (e.g. Brown et al., 2002; Kounov et al., 2008, 2009; Raab et al., 2002; Tinker et al., 2008). The third box allows for the modeling of possible thermal events in the Cenozoic.

The models reveal a period of accelerated cooling through 120 to 40 °C (the limits of the partial annealing zones for apatite fission-track and (U–Th–[Sm])/He thermochronological methods, Fig. 7) between 100 and 65 Ma. To define precisely the time of the cooling event for each modeled sample we use the "weighted mean" path, which we consider as the most probable thermal history. The more commonly used "best fit" path is only the statistically best fitting path but not necessarily the most realistic geological solution.

4. Discussion

4.1. Paleozoic evolution

Although only based on three samples, the fact that sample AG09, the topographically lowest of the Augrabies section (546 m), has a ZFT age (367 ± 23 Ma) younger than samples from higher altitude – AG01 (848 m, 439 ± 49 Ma) and AG06 (840 m, 420 ± 50 Ma) – suggests that the study area cooled down monotonically as one coherent block between ~439 and ~367 Ma (Fig. 6). The age and altitude differences between these samples indicate about 300 m of denudation over a period of more than 140 myr (Figs. 2 and 6). While this positive age–altitude trend is hardly tenable on the basis of only those three samples, the idea that they underwent very slow cooling as derived from their age–altitude relationship is also supported by the dispersion of the single grain ages (Fig. 9). High dispersion is generally indicative of slow cooling or partial resetting (e.g. Fügenschuh and Schmid, 2003). At slow cooling rates, the difference in the individual closure temperature of the single zircon grains becomes more important than in the case of rapid cooling/exhumation, due to the possibly different kinetic parameters of each grain (e.g. Kasuya and Naeser, 1988).

Our zircon central fission-track ages (AG09 — 367 ± 23 Ma, AG01 — 439 ± 49 Ma and AG06 — 420 ± 50 Ma) do not correspond to any previously reported phase of accelerated cooling, denudation or thermal event in Southern Africa. This corroborates the conclusion that these ages only represent a phase of very slow, continuous cooling in the study area following the Late Ediacaran to Early Cambrian Pan-African orogeny. In addition we can also conclude that even the Pan-African orogeny did not generate temperatures higher than 200–250 °C in the Augrabies area, as shown by single grains with older, Early Neoproterozoic ages (sample AG01, Fig. 9; note the relatively large error).

Although a general slow cooling in the area seems plausible for the regional post-Pan-African evolution, some zircon fission-track and He ages may nevertheless also indicate a discrete period of enhanced cooling. The ZFT age of sample AG09 (367 ± 23 Ma) and the ZHe age

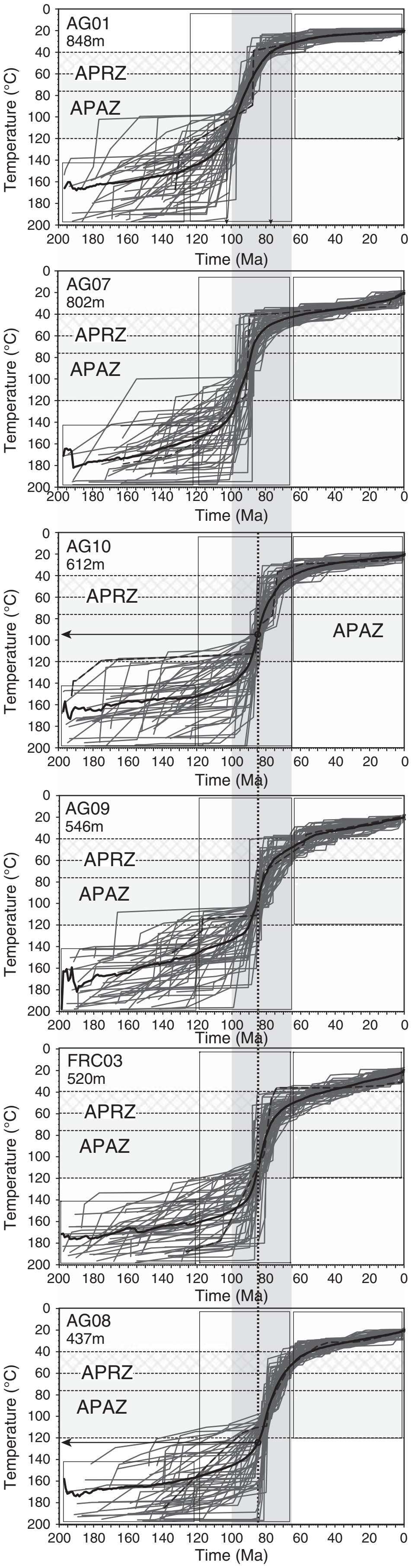

Fig. 7. Modeled thermal histories of the dated samples. Thin black rectangles are user-defined time (t) — temperature (T) boxes. Bracketed between 40–75 °C is the (U–Th–[Sm])/He partial retention zone (APRZ) for apatite as defined by Farley (2000). Bracketed between 60–120 °C is the fission-track partial annealing zone for apatite (APAZ) as defined by Laslett et al. (1987). Black dashed lines represent the best fit paths of the modeled thermal history, while the gray lines represent 50 "good" thermal history paths corresponding to a goodness of fit value >0.5 (for details see the text). Thick black lines represent "weighted mean" paths.

of sample AG02 (342 ± 55 Ma), for example, may prove a period of increased denudation in the Augrabies area. This event can be linked to the regional uplift marked by the stratigraphic hiatus of Carboniferous age that separates the Cape Supergroup from the overlying Karoo Supergroup (Fig. 10, Catuneanu et al., 2005; Visser, 1990). It is possible that our data unveil the only evidence so far for the onset of the uplift phase of the source area of the Cape Basin, potentially synchronous with the Mid Devonian–Early Carboniferous accelerated subsidence of the basin itself promoted by extensive normal faulting (Tankard et al., 2009).

4.2. Late Carboniferous–Early Permian evolution

The glacigene Dwyka Group (Upper Carboniferous–Lower Permian) sediments are exposed in the northeastern corner of the Augrabies area (Fig. 5). They onlap the underlying metamorphic basement at a present-day altitude of between 800 and 850 m. This requires that the underlying metamorphic sequence was already exposed during the Late Carboniferous, as supported by the ZHe age of sample AG02 (342 ± 55 Ma, 675 m), which shows that the area was exhumed to temperatures below 180 °C already by the Early Carboniferous. However, this conclusion seems to be contradicted by the younger ZHe age of sample AG09 (237 ± 62 Ma, 546 m). If the above scenario is true and indeed sample AG02 was at, or near to, the surface during the Early Carboniferous, the fact that the age of sample AG09 is younger than the Dwyka sedimentation episode suggests that during the deposition of this unit the temperature was higher than 180 °C at a depth of 250 m (altitude difference between samples AG02 and 09). Given that this would require an impossible thermal gradient, we have to conclude that the present day surface, as exposed elsewhere than at the contact with the base of the Dwyka, was not exposed during the Early Carboniferous. Moreover, although we do not know the actual Carboniferous and Permian thermal gradient, there must have been substantial relief to heat the rock section above sample AG09 to temperatures higher than 180 °C. Burial of the sample to such a temperature below Dwyka sediments or a thermal event during the Permian or the Early Triassic is not suggested by any known independent evidence, including the insufficient thickness of Dwyka Group deposits. We support, therefore, the model that during the evolution of the Karoo Basin the study area belonged to the topographic high called Cargonian Highland (e.g. Veevers et al., 1994). A high relief in the study area during the Late Carboniferous–Early Permian could explain the observed difference in the ZHe ages. Sample AG09 was covered possibly by a significant overburden and experienced temperatures above the closure temperature of the ZHe system. Sample AG02, some 20 km away and 250 m higher up (Fig. 5), was however situated just below this temperature. The continental Dwyka sediments that presently crop out more than 80 km away from sample AG09 were then probably deposited in low relief areas far away from the Cargonian Highland.

4.3. Cretaceous denudation

Our study does not provide constraints on the thermal evolution of the areas of interest between the Late Triassic and the Early Cretaceous. The area was possibly covered by Karoo Supergroup sedimentary rocks and by the Lower Jurassic flood basalts of the Drakensberg Group

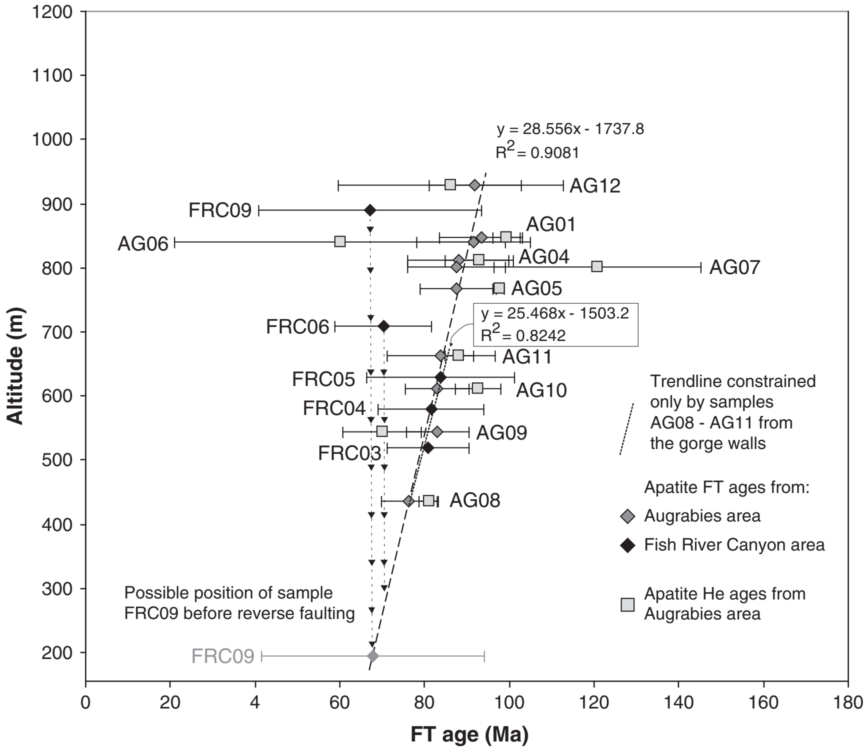

Fig. 8. AHe and AFT ages vs. elevation plots from the studied areas.

(184–174 Ma; Jourdan et al., 2007) in addition to the dolerite sills that crop out extensively in the Karasburg and Main Karoo Basins (Fig. 2). Certainly though the region was at temperatures higher than 120 °C before the Late Cretaceous, when the region experienced accelerated cooling, as suggested by the thermal modeling of the samples (100–65 Ma, Fig. 7; see also Kounov et al., 2009). Late Cretaceous accelerated cooling and significant denudation have been already reported from the South African margin and from its interior (115–80 Ma, e.g., Brown et al., 2000; Flowers and Schoene, 2010; Kounov et al., 2009; Tinker et al., 2008). A significant amount of denudation is also observed offshore Namaqualand, where seismic profiles and boreholes show erosional horizons marking the Aptian regression (121–112 Ma, e.g. Aizava et al., 2000; Brown et al., 1995; Gerrard and Smith, 1983). Margin uplift was locally related to active tectonics accompanied by denudation (Brown, 1992; Kounov et al., 2009; Raab et al., 2002).

Apatite fission-track ages between 99 and 73 Ma, similar to ours, were reported by Brown et al. (1990) from elsewhere along the Fish River and Orange Rivers basins. Our study area and those sampled by Brown et al. (1990) coincide with the western termination of the so-called Etosha–Griqualand–Transvaal epeirogenic flexure axis (Fig. 1, Du Toit, 1926; Moore, 1999). The inferred age of flexure, based on apatite fission-track data, is Late Cretaceous (Moore, 1999). The Late Cretaceous is also the time of the increase in sediment supply from the Orange River system (Dingle and Hendey, 1984; Dingle and Robson, 1992) and of the Campanian–Maastrichtian high sedimentation rate recorded in the offshore Orange Basin (Rust and Summerfield, 1990).

The accelerated cooling documented by apatite fission-track data can therefore be explained by the increased erosion rates in the Orange and Fish River basins (Brown et al., 1990). Accelerated erosion was possibly linked to substantial regional uplift. However, whereas this event is readily explained for the continental margin setting, it remains conceptually challenging for the continental interior. Some authors relate post-break-up tectonic processes in Southern Africa to dynamic processes in the mantle (e.g. Burke, 1996; de Wit, 2007; Doucouré and de Wit, 2003; Kounov et al., 2009; Tinker et al., 2008). Substantial uplift is associated spatially with the tomographically-imaged low-velocity zone in the lower mantle–core boundary, called the African Superplume (e.g. Lithgow-Bertelloni and Silver, 1998). According to this model, the present-day topography would be a dynamic feature formed in response to vertical stresses at the base of the southern African lithosphere that generated positive buoyancy in the mid-lower mantle (Burke, 1996; Ebinger and Sleep, 1998; Gurnis et al., 2000; Lithgow-Bertelloni and Silver, 1998; Nyblade and Robinson, 1994). Periods of increased denudation are also correlated with peaks of kimberlite emplacement, thus suggesting a causative link between lower-mantle upwelling processes and increased denudation. Certainly, peaks of kimberlitic activity were related to the emplacement of hot magma at the base of the lithosphere, which triggered diffuse uplift. Indeed, modeled mantle density and viscosities (Gurnis et al., 2000) assume the Cretaceous uplift in Southern Africa to be plume-related.

Sub-continent-scale uplift was also accompanied by localized tectonic activity, mostly related to reactivation of preexisting extensional fault structures along the continental margin (e.g. Viola et al., 2005). In general, though, the offset of Proterozoic features across Cretaceous faults is minimal, which excludes tectonic reworking of regional significance of the study areas. An example of localized faulting along the Fish River Canyon is illustrated in Fig. 3b, which shows the reverse offset of the Nama sedimentary strata and of the NMP–Nama nonconformity across a steeply E-dipping fault. Sample FSC09, from the top of the dated section (890 m) within the hanging wall of the fault, yielded an AFT age of 67 ± 26 Ma, and is thus younger than the samples from the footwall (Fig. 4, 84–81 Ma), confirming the reverse movement along the fault. If sample FRC09 is plotted back to its inferred pre-faulting position on the interpolated age–altitude linear trend of Fig. 8, we can constrain ~700 m of vertical throw. Restoring the sample and the hanging wall back to this position, however, would also lead to the normal offset of the nonconformity between NMP gneisses and Nama Group sediments by several hundred meters. This leads us to

Table 3
(U–Th–[Sm])/He analysis results from the Augrabies Falls area.

Sample	Aliq.	He vol. [ncc]	He s.e. [ncc]	U238 mass [ng]	U238 s.e. [ng]	Th232 mass [ng]	Th232 s.e. [ng]	Th/U Ratio	Sm mass [ng]	Sm s.e. [ng]	Ejection correct. (Ft)	Uncorr. He-age [Ma]	Ft-Corr. He-age [Ma]	2 s [Ma]	Sample unweighted aver. (2 s.e.)	
Apatite																
AG01	#1	13.068	1.7	1.051	1.8	1.487	2.4	1.41	1.097	13.5	0.755	76.2	100.9	8.6		
	#2	2.548	1.7	0.244	1.8	0.301	2.4	1.23	0.290	13.6	0.680	66.1	97.1	10.3		
	#3	2.416	1.7	0.225	1.8	0.264	2.4	1.18	0.224	13.8	0.718	68.9	96.0	9.2		
	#4	3.771	1.7	0.361	1.8	0.316	2.4	0.88	0.378	13.9	0.696	70.8	101.7	10.3	**98.9**	**3.2**
AG04	#1	1.177	1.9	0.097	1.9	0.077	2.5	0.79	2.429	15.3	0.801	*71.9*	89.8	7.9		
	#5	0.369	2.2	0.028	2.5	0.025	2.7	0.92	1.003	16.2	0.758	*72.4*	95.5	10.6	**92.6**	**8.1**
AG05	#1	0.295	2.5	0.034	2.4	0.007	4.2	0.20	0.117	20.0	0.692	*67.2*	97.1	11.1		
	#3	0.081	3.7	0.012	4.7	0.002	7.5	0.15	0.067	20.6	0.518	*50.7*	97.8	18.0	**97.5**	**1.0**
AG06	#1	0.148	2.7	0.018	3.2	0.074	2.5	4.12	0.184	13.4	0.721	*33.1*	45.9	4.9		
	#2	0.292	2.3	0.009	5.4	0.088	2.5	9.60	0.800	13.4	0.668	*65.5*	98.1	12.4		
	#3	0.210	2.5	0.032	2.3	0.121	2.5	3.74	0.357	13.5	0.772	*27.1*	35.0	3.2	**59.7**	**39.0**
AG07	#1	4.201	1.7	0.164	1.8	0.818	2.4	5.00	1.327	18.3	0.624	*93.9*	150.4	18.3		
	#2	2.748	1.7	0.124	1.9	0.680	2.4	5.47	1.211	18.6	0.729	*76.7*	105.2	9.9		
	#3	2.123	1.7	0.107	1.9	0.488	2.4	4.58	1.126	18.8	0.690	*75.6*	109.6	11.5		
	#4	1.793	1.8	0.083	1.9	0.463	2.4	5.54	0.958	19.0	0.719	*73.6*	102.3	10.0		
	#5	1.703	1.8	0.071	2.0	0.272	2.4	3.83	1.334	19.8	0.712	*95.9*	134.8	13.8	**120.5**	**24.4**
AG08	#1	1.182	1.9	0.140	1.9	0.171	2.4	1.23	1.411	16.4	0.647	*50.8*	78.6	9.2		
	#2	6.962	1.7	0.608	1.8	0.968	2.4	1.59	5.415	16.6	0.786	*65.1*	82.8	6.6		
	#3	2.641	1.7	0.282	1.8	0.345	2.4	1.22	2.638	16.8	0.691	*56.6*	81.9	8.6		
	#4	2.356	1.7	0.232	1.8	0.392	2.4	1.69	2.601	17.0	0.706	*56.1*	79.4	8.0	**80.7**	**2.3**
AG09	#1	0.635	1.9	0.077	1.9	0.141	2.5	1.83	0.969	5.4	0.698	*44.3*	63.4	6.5		
	#2	6.422	1.7	0.615	1.8	0.863	2.4	1.40	4.344	17.2	0.820	*61.9*	75.5	5.3		
	#3	5.464	1.7	0.407	1.8	1.010	2.4	2.48	4.040	17.7	0.819	*66.3*	81.0	5.8		
	#4	0.926	1.9	0.104	1.9	0.178	2.4	1.72	1.137	17.9	0.750	*49.1*	65.4	5.9		
	#5	1.306	1.8	0.159	1.8	0.239	2.4	1.50	1.368	18.1	0.748	*47.4*	63.4	5.7	**69.7**	**9.3**
AG10	#1	7.051	1.7	0.700	1.8	0.276	2.4	0.39	3.726	4.5	0.747	*72.9*	97.6	8.6		
	#2	1.887	1.7	0.204	1.8	0.071	2.5	0.35	1.536	4.4	0.733	*66.6*	90.9	8.4		
	#4	1.835	1.7	0.204	1.8	0.061	2.5	0.30	1.376	7.0	0.743	*65.8*	88.6	8.0	**92.3**	**5.4**
AG11	#2	17.945	1.7	1.398	1.8	3.552	2.4	2.54	5.908	14.8	0.761	*64.7*	84.9	7.1		
	#3	11.108	1.7	0.910	1.8	1.997	2.4	2.20	4.531	15.0	0.733	*64.5*	87.9	8.0		
	#4	6.768	1.7	0.582	1.8	1.318	2.4	2.26	2.466	15.1	0.674	*61.0*	90.6	9.7	**87.8**	**3.3**
AG12	#1	0.348	2.1	0.026	2.6	0.038	2.6	1.46	0.154	14.0	0.736	*79.3*	107.7	10.6		
	#2	0.496	2.1	0.066	2.0	0.095	2.5	1.44	0.431	14.1	0.719	*44.4*	61.8	6.1		
	#3	1.325	1.8	0.119	1.9	0.157	2.4	1.32	1.559	14.3	0.738	*64.8*	87.8	8.2	**85.8**	**26.6**
Zircon																
AG02	#2	81.711	1.6	2.353	1.8	0.515	2.4	0.22	0.198	12.7	0.738	*266.9*	361.7	33.0		
	#3	78.140	1.6	2.495	1.8	0.501	2.4	0.20	0.022	13.0	0.751	*242.4*	322.6	28.4	**342.1**	**55.2**
AG09	#1	34.736	1.6	1.136	1.8	0.791	2.4	0.70	0.044	6.1	0.741	*213.5*	288.1	25.8		
	#2	44.846	1.6	2.774	1.8	0.761	2.4	0.27	0.209	5.5	0.688	*124.4*	180.8	18.9		
	#3	44.087	1.6	2.094	1.8	0.481	2.4	0.23	0.141	5.5	0.672	*163.0*	242.5	26.4	**237.2**	**62.2**

Amount of helium is given in nano-cubic-cm in standard temperature and pressure. Amount of radioactive elements is given in nanograms. Ejection correct. (Ft): correction factor for alpha-ejection (according to Farley et al., 1996; Hourigan et al., 2005). Uncertainties of helium and the radioactive element contents are given as 1 sigma, in relative error %. Uncertainty of the single grain age is given as 2 sigma in Ma and it includes both the analytical uncertainty and the estimated uncertainty of the Ft. Uncertainty of the sample average age is 2 standard error, as (SD)/(n)1/2; where SD = standard deviation of the age replicates and n = number of age determinations.

the conclusion that a pre-thrusting top–down-to-the east normal faulting component of several hundred meters was accommodated along the same fault.

Plotting the second outlier, sample FRC06 (70 ± 11 Ma, 710 m), on the age–altitude trend line (Fig. 8) does not lead to satisfactory results because the altitude difference with sample FRC09 would become less

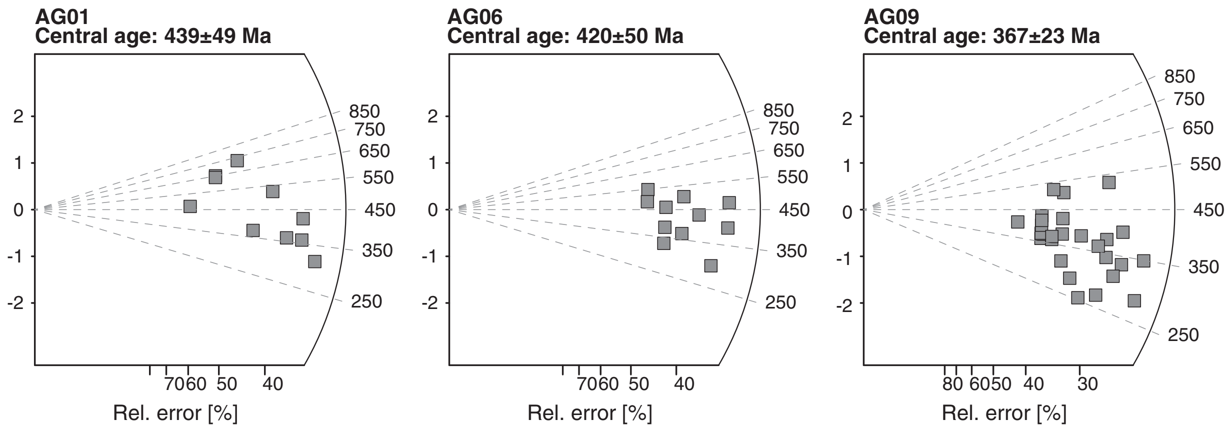

Fig. 9. Radial plots of zircon fission-track ages (Galbraith, 1990).

than 100 m, thus in stark contrast to the present day difference of about 180 m. This confirms the field observation that sample FRC06 is not part of the hanging wall but belongs to the fault zone core. Its age can therefore be tentatively taken as the age of the reverse faulting episode, due to the effects of age resetting in response to the thermal anomaly along the fault zone (e.g. Viola and Anczkiewicz, 2008). It cannot be excluded that the age of sample FRC09, although only poorly constrained due to its large error, is also related to the age of the actual faulting event, during which the sample was exhumed rapidly to depths above the closure temperature of the apatite FT system.

We note that Raab et al. (2002) also suggested a period of accelerated cooling beginning at about 70 Ma in central Namibia related to the reverse reactivation of earlier basement structures (e.g. the Waterberg thrust). Caution is nonetheless necessary with our interpretation, given that hydrothermal processes along this weak fault zone continue even today, as documented by the hot springs in the area.

If not directly linked to localized active tectonics, uplift in the cratonic interior is therefore regional. It should be noted that apatite fission track ages reported in the literature from the other parts of the craton (i.e. Main Karoo Basin) are higher (169–111 Ma, Brown et al., 1990; Tinker et al., 2008; Kounov et al., 2008, 2009). Enhanced erosion along the Fish and Orange River probably caused a component of isostatic rebound (e.g. Simpson, 2004; Zeilinger et al., 2005), which led to additional uplift, which might explain the younger fission-track ages along these rivers in comparison to the surrounding areas, despite similar current altitudes. During the Cretaceous, the Fish and Orange River basins were probably part of the greater Kalahari River catchment area (de Wit, 1999).

It has to be noted, however, that the time of the accelerated cooling history constrained by our study in the Late Cretaceous (100–65 Ma) corresponds also to important episodes of alkaline intrusions (e.g. kimberlites) in the region (Fig. 10, Jelsma et al., 2004; Moore et al., 2008). The younger ages from those areas can therefore be also related to those events.

Recently, Moore et al. (2009) drew attention to major inconsistencies between the present topography of Southern Africa and the expected dynamic topography predicted by plume-based models. They proposed that the drainage network of Southern Africa, which is characterized by river divides broadly parallel to the continent coastline, is strongly incompatible with the broad dome and radial drainage patterns predicted by models, which link genetically the elevated average altitude of Southern Africa to uplift over a deep mantle plume. The ages of these drainage divides, which they interpreted as axes of epeirogenic uplift, are correlated with major reorganizations of spreading regimes in the oceanic ridges surrounding Southern Africa, suggesting an origin from stresses related to plate motion (Moore et al., 2009). One of these river divides corresponds to the previously mentioned Etosha–Griqualand–Transvaal flexural axis (Fig. 1). Its formation during the Late Cretaceous corresponds to a well-known major shift in pole rotation of the African/South American plates (e.g. Nürnberg and Müller, 1991).

4.4. Paleorelief

Although no solid conclusion can be drawn as yet as to the driving forces of the Late Cretaceous uplift/denudation that affected Southern Africa, we can at least speculate about the paleorelief of the region at that time based on the fission-track age pattern obtained in this study. As shown above, the accelerated cooling that affected the region was triggered by regional uplift (and not distinct tectonic episodes). Denudation can, therefore, be considered to be the direct consequence of the increased river gradients due to regional uplift. The development of relief along the South African margin and interior during the Cretaceous has been already suggested by several authors (e.g. Brown et al., 2000; Kounov et al., 2008, 2009; Tinker et al., 2008). The fact that fission-track ages from the flat part of the Augrabies transect are similar and, together with those derived from the gorge samples show a positive age–altitude trend with a slope comparable to that obtained from the Augrabies gorge (samples AG08–11, Figs 5 and 8) and the Fish River Canyon (samples FRC03–05, Figs. 4 and 8), suggests that the erosion rate was similar over the whole study area. Similar age — altitude gradients from all our sections suggest therefore that an irregular paleosurface did not disturb subsurface isotherms (e.g. Braun, 2005; Stüwe et al., 1994) and thus we can

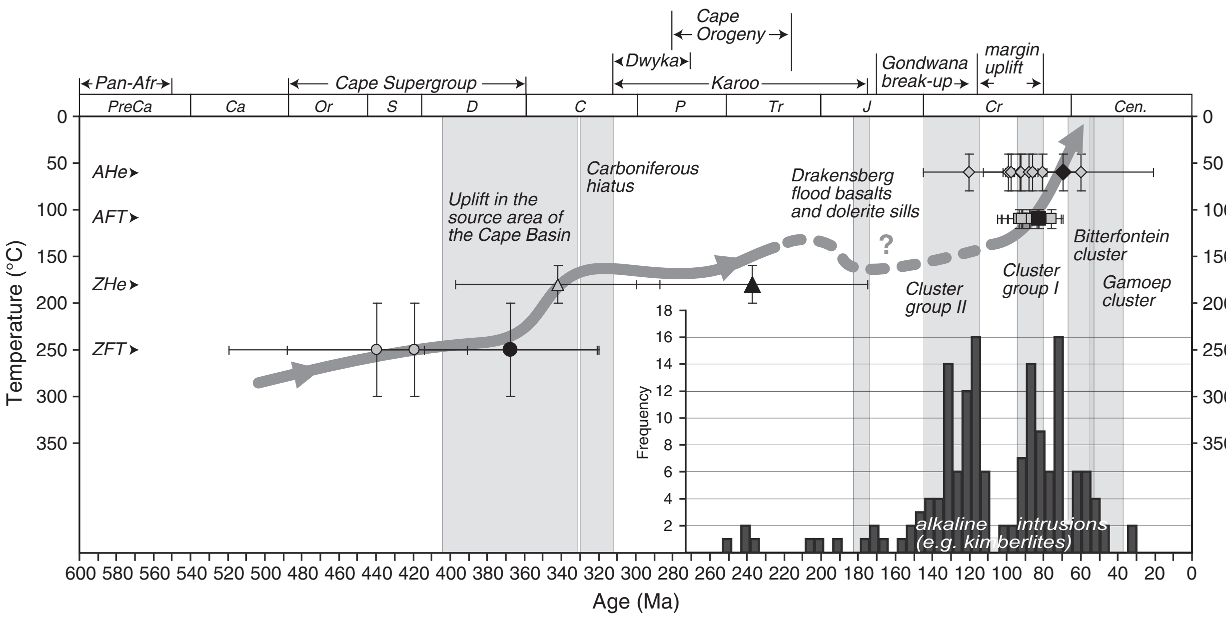

Fig. 10. Compilation of the major relevant events of the geological evolution of Southern Africa integrated with the derived low-temperature evolution of the study area. The frequency diagram compiles available age data of Southern African kimberlites (Jelsma et al., 2009). Vertical error bars of the dated samples represent the partial annealing zones of 200 to 300 °C for ZFT, 120 to 60 °C for AFT and partial retention zones of 200 to 160 °C for ZHe and 75 to 40 °C for AHe thermochronometers (Green and Duddy, 1989; Reiners, 2005). Black symbols represent the different low-temperature thermochronological results of sample AG9.

exclude sharp Alpine-type relief including deeply incised valleys and steep hill slopes (House et al., 1998, 2001; Reiners et al., 2003). The derived elevated Cretaceous erosion rates would be unlikely without wet climatic conditions (Partridge, 1998).

A high relief mountain range (highly erodable) probably formed instead along the present day escarpment area, where the available AFT patterns demonstrate how the subsurface isotherms were clearly affected by topography (Kounov et al., 2008).

4.5. Estimation of the Paleozoic and the Mesozoic denudation rates

Different thermochronological methods (ZFT, ZHe, AFT and AHe) applied to the same sample make it possible to estimate the cooling and denudation rates for a wide range of temperatures and time intervals. Modeling of the AFT and AHe data provides information about cooling rates trough the temperatures corresponding to the apatite partial annealing zones for both fission-track and (U–Th–[Sm])/He methods (120–40 °C). By using the "weighted mean" path from the model of sample AG01 (Fig. 7), we derive a cooling rate of 3.2 °C/myr for the 102–77 Ma time span. Although this cooling rate cannot be converted into a denudation rate due to the unknown thermal gradient at that time, a tentative denudation rate of 160 and 107 m/myr can be calculated for two arbitrary thermal gradients of 20 and 30 °C/km, respectively. Similar cooling rates were also derived from the models of the other analyzed samples.

By using the samples from the vertical section from the Orange River gorge (samples AG08–10, Figs. 6 and 8) we can calculate the thermal gradient for a given time interval starting from the estimated temperatures of the lowest and highest sample at that time. This is based on the assumption that the samples preserved their original position in the rock column and were not displaced vertically by later faults. This is indeed the case of the study area as explained before. The calculation yields abnormally high thermal gradients. For example, from the couplet of samples AG08 and AG10 at 85 Ma a thermal gradient of 166 °C/km is calculated (Fig. 7). It can therefore be concluded that the modeling of both fission-track and (U–Th–[Sm])/He data yields unrealistically high thermal gradients, despite the fact that at that time (~85 Ma ago) significant kimberlitic activity occurred in the area and a relatively elevated thermal gradient can therefore be expected. We anticipate that the calculated cooling and denudation rates from the models are overestimated. Elevated cooling rates are calculated from the thermal modeling because of overlapping AFT and AHe ages, which suggests cooling at the same time through both the AFT and AHe partial annealing temperatures (120–40 °C). We believe that these cooling rates are exaggerated due to the expected higher closure temperatures for the AHe system. Recent laboratory experiments with natural apatites show that the He effective closure temperature increases with decreasing cooling rates (Flowers et al., 2009; Shuster et al., 2006). Therefore the AHe system might have closure temperatures as high as the AFT in areas characterized by rather slow cooling rates, which is indeed the case of the study area (Flowers et al., 2009).

A second possibility to derive direct estimates of denudation rates is provided by the slope of the age — altitude curve obtained from the AFT samples. A prerequisite is that all the samples had the same closure temperature and that there was no thermal relaxation in the area, which would depress the isotherms.

For samples AG08 to AG11, which come from the wall of the Orange River gorge (where the influence of the paleorelief can be excluded due to the very little lateral distance between the samples), we obtain a regression line with a very high R^2 value (coefficient of determination). The slope of this line constrains a denudation rate of 25.5 m/myr. We consider this denudation rate more realistic than that obtained from the thermal modeling, although minor thermal relaxation following the peak of the kimberlitic activities at that time cannot be excluded.

It has to be stressed that our estimated denudation rate is an order of magnitude higher than the present-day denudation rates derived from cosmogenic isotope studies (e.g. Cockburn et al., 2000; Kounov et al., 2007). Nonetheless, the Late Cretaceous rates are still relatively low in absolute terms and are most probably related to enhanced erosion under wet climatic conditions (Partridge, 1998) due to regional uplift and not to localized tectonic activity.

Despite the small number of data points and the fact that the samples are collected from a relatively large area (thus making the influence of the paleorelief on the age — altitude plot possible), loosely constrained figures of the denudation rates during the Early Silurian–Late Devonian (439 to 367 Ma) and the Carboniferous–Mid Triassic interval (342 to 237 Ma) can be calculated from the new ZFT and ZHe data (Fig. 6). A denudation rate of 4.5 m/myr is derived for the Early Silurian to Late Devonian interval and 1.2 m/myr for the Carboniferous to Mid Triassic. These very slow rates are compatible with those obtained for the present day surface of the same areas (Cockburn et al., 2000; Kounov et al., 2007).

It must be mentioned that the zircon FT and He ages could be also affected by the accumulation of alpha damage in the crystal lattice, which has a strong control on the closure temperature (e.g. Garver et al., 2002; Rahn et al., 2002; Reiners, 2005). Thereby, the grains with higher uranium content that accumulated more alpha damages have a lower closure temperature and consequently yield relatively younger ages. Such a situation was probably not the case in our study because there is no correlation between age and U content for the zircon FT (Appendix C) and He (Table 3) single grain ages.

5. Conclusions

New ZFT and ZHe thermochronological results suggest that at least the western part of the southern African cratonic interior in general cooled down monotonically as one coherent block from the Early Silurian to the Mid Triassic, with very low denudation rates of between 1.2 and 4.5 m/myr. These very slow rates are comparable with those obtained for the present day surface of the same areas (Cockburn et al., 2000; Kounov et al., 2007). Although a regional slow cooling in the area seems reasonable for the post-Pan-African evolution, some zircon fission-track and He ages can nevertheless reflect a discrete period of enhanced cooling during the Mid Devonian–Early Carboniferous, which we tentatively correlate to the major hiatus that separates the Cape Supergroup from the overlying Karoo Supergroup (Fig. 10).

During the Late Carboniferous–Early Permian the Augrabies and the Fish River Canyon areas were probably part of the high and dry land called the Cargonian Highland (e.g. Veevers et al., 1994).

Joint modeling of apatite fission-track and (U–Th–[Sm])/He data reveals a period of accelerated cooling through 120 to 40 °C between 100 and 65 Ma ago (Fig. 10). The accelerated cooling was most probably the direct consequence of regional uplift, in combination with high river gradients and consequent enhanced erosion rates and denudation in the Orange and Fish Rivers basins, which, during the Cretaceous, were probably part of the greater Kalahari River catchment area (de Wit, 1999).

A denudation rate of 25.5 m/myr was calculated for the Late Cretaceous from the slope of the AFT age–altitude curve (Fig. 7). Although higher than the present-day rates for the same region, these rates are relatively low and related most probably to enhanced erosion and regional uplift rather than tectonic activity. These denudation rates can be overestimates due to the possible thermal relaxation following the maximum of kimberlitic magmatism in the Late Cretaceous. The elevated average altitude in the area during the Late Cretaceous was probably not related to the formation of a pronounced Alpine-type relief with deep valleys and steep hill slopes.

Acknowledgments

This study was partially financed by the NGU and Statoil through "The African Plate" project and forms part of the DFG Priority Programme "SAMPLE: South Atlantic Margin Processes and Links with onshore Evolution". Constructive reviews by Marc Jolivet and Diane Seward helped to improve the quality of the paper. We would like to thank the staff of the Augrabies Falls National Park for their support during the sampling campaign within the national park. We are indebted to Jodie Miller and Chris Le Coq for their hospitality and to Maarten de Wit and Ivan Wilson for their support and assistance.

Appendix A. Fission track thermochronology

Whole rock samples were crushed and apatite and zircon grains were recovered by conventional heavy liquid and magnetic methods. Apatite grains were mounted in epoxy resin, polished and etched with 5.5 N HNO_3 at 21 °C for 20 s. Zircon grains were etched in an eutectic mixture of KOH and NaOH at 220 °C for between 10 and 24 h. Irradiation was carried out at the OSU facility, Oregon State University Radiation Center, USA. Microscopic analysis was completed at Basel University using an optical microscope with a Kinetek computer-driven stage (Dumitru, 1995). The magnification used was ×1250 for apatite and ×1600 (dry objective) for zircon. All ages were determined using the ζ approach (Hurford and Green, 1983) with a ζ value of 332 ± 7 for apatite (CN5 standard glass) and 122 ± 2 for zircon (CN1 standard glass) (Table 1, analyst: A. Kounov). The ages are reported as central ages (Galbraith and Laslett, 1993) with a 2σ error (Table 1). Horizontal confined track lengths in apatite grains were measured at a magnification of ×1250. Fission-track etch-pit diameters (Dpar) were measured at a magnification of ×1250 in order to estimate the compositional influence on fission track annealing (Carlson et al., 1999).

The temperatures at which fission tracks in apatite and zircon partially anneal (i.e. partial isotopic resetting) are not sharply defined. The temperature range within which partial track annealing occurs is known as the partial annealing zone (PAZ). The effective closure of the system lies within this PAZ and depends on overall cooling rate and kinetic properties of the host mineral. The specific partial annealing zone for apatite lies between 60 and 120 °C (Corrigan, 1993; Green and Duddy, 1989), with a mean effective closure temperature of 110 ± 10 °C (Gleadow and Duddy, 1981).

Unfortunately, our knowledge of zircon annealing is less advanced and a wide-range of temperature intervals has been published for the partial annealing zone of zircon. Yamada et al. (1995) suggested temperature limits of ~390–170 °C, whereas Tagami and Dumitru (1996) and Tagami et al. (1998) suggested temperature limits of ~310–230 °C. Recently, in his overview on the zircon fission track dating method, Tagami (2005) reported temperature ranges for the closure temperature between ~300–200 °C. Accordingly, we use a value of 250 ± 50 °C for the mean effective closure temperature and the 200–300 °C temperature interval for the partial annealing zone.

Appendix B. (U–Th–[Sm])/He thermochronology

The (U–Th–[Sm])/He technique is a relatively young low-temperature thermochronological method that is typically used for the reconstruction of the thermal history of the upper crust. The major advantage of this thermochronometer is that the different minerals yield even lower closure temperatures than the fission-track method (e.g. Farley, 2002; Reiners, 2005). The He thermochronology is based on the alpha-decay of the natural radioactive isotopes of ^{238}U, ^{235}U, ^{232}Th and ^{147}Sm. Apatite and zircon are the most commonly dated minerals, and therefore their crystallography, mineral chemistry and diffusion parameters are the best studied (e.g. Farley, 2000; Reiners, 2005). The selection criteria of the individual grains for analysis are very strict and only intact crystals with no any visible inclusions should be dated. Fluid inclusions may contain helium from hydrothermal fluids and the amount of excess helium due to this source is undistinguishable from the radiogenic helium which would lead to the increase of the (U–Th–[Sm])/He age. Other biasing factors are the size and shape of the crystal, the internal zoning and the variation of the U/Th ratio. Fractures and open cleavages act as diffusion channels and can contribute to the increase of the surface-area-to-volume ratio. Helium is an extremely mobile element and it has a high diffusion rate in most solid phases. That is why the closure temperatures in different minerals are low (in zircon and in apatite it is around 185 and 75 °C at cooling rate of 1 °C/myr, respectively, Farley et al., 2002; Reiners et al., 2002, 2004). The closure temperature (Wolf et al., 1998) depends mainly (i) on the diffusivity of helium in the lattice of the mineral, (ii) on the dimensions of the diffusion domain (= usually the size of the dated crystal), (iii) on the cooling rate, and (iv) on the radiation damage density of the crystal lattice. Similarly to other methods (e.g. fission track) the closure temperature is not a sharp boundary. The degree of diffusive loss of helium depends on the temperature and the effective heating time. Consequently there is mineral and method specific "partial retention temperature zone" (PRZ), where the accumulation of helium is not proportional to time. In apatite, for example in the temperature range between 75 °C and ca. 40 °C at cooling rate of 1 °C/myr, part of the continuously forming He gas diffuses out of the crystal within a few million years (Farley, 2000). The partial retention zone for the zircon is in the range of 200 to 160 °C (e.g. Reiners, 2005).

Appendix C. Supplementary data

Supplementary data to this article can be found online at http://dx.doi.org/10.1016/j.tecto.2013.05.009.

References

Aizava, M., Bluck, B., Cartwright, J., Milner, S., Swart, R., Ward, J., 2000. Constrains on the geomorphological evolution of Namibia from the offshore stratigraphic record. Communes of the Geological Survey of Namibia 12, 337–346.

Andreoli, M.A., Doucoure, M., Van Bever Donker, J., Brandt, D., Andersen, N.J.B., 1996. Neotectonics of Southern Africa — a review. Africa Geoscience Review 3, 1–16.

Basson, I.J., Viola, G., 2003. Structural overview of selected Group II kimberlite dyke arrays in South Africa: implications for kimberlite emplacement mechanisms. South African Journal of Geology 106, 375–394.

Basson, I.J., Viola, G., 2004. Passive kimberlite intrusion into actively dilating dyke-fracture arrays: evidence from fibrous calcite veins and extensional fracture cleavage. Lithos 76, 283–297.

Braun, J., 2000. Quantitative constraints on the rate of landform evolution derived from low-temperature thermochronology. In: Reiners, P.W., Ehlers, T.A. (Eds.), Low-temperature Thermochronology: Techniques, Interpretations, and Applications. Reviews in Mineralogy and Geochemistry, 58, pp. 351–374.

Brown, L.F., Benson, J.M., Brink, G.J., et al., 1995. Sequence stratigraphy in offshore South African divergent basins, an atlas on exploration for cretaceous lowstand traps by SOEKOR (Pty) Ltd. AAPG Studies in Geology 184, 41.

Brown, R.W., 1992. A Fission Track Thermochronology Study of the Tectonic and Geomorphic Development of the Sub-aerial Continental Margins of Southern Africa. (PhD thesis) La Trobe University, Melbourne, Australia.

Brown, R.W., Rust, D.J., Summerfield, M.A., Gleadow, A.J.W., de Wit, M.C.J., 1990. An Early Cretaceous phase of accelerated erosion on the south-western margin of Africa: evidence from apatite fission track analysis and the offshore sedimentary record. Nuclear Tracks and Radiation Measurement 17, 339–350.

Brown, R.W., Gallagher, K., Gleadow, A.J.W., Summerfield, M.A., 2000. Morphotectonic evolution of the South Atlantic margins of Africa and South America. In: Summerfield, M.A. (Ed.), Geomorphology and Global Tectonics. John Wiley and Sons Ltd, pp. 255–284.

Brown, R.W., Summerfield, M.A., Gleadow, A.J.W., 2002. Denudation history along a transect across the Drakensberg Escarpment of southern Africa derived from apatite fission track thermochronology. Journal of Geophysical Research 107. http://dx.doi.org/10.1029/2001JB000745.

Burke, K., 1996. The African Plate. South African Journal of Geology 99, 341–409.

Burke, K., Gunnell, Y., 2008. The African erosion surface: a continental-scale synthesis of geomorphology, tectonics, and environmental change over the past 180 million years. Geological Society of America, Memoir 201, 66.

Carlson, D.W., Donelick, R.A., Ketcham, R.A., 1999. Variability of apatite fission-track annealing kinetics, I. Experimental results. American Mineralogist 84, 1213–1223.

Catuneanu, O., Wopfner, H., Eriksson, P.G., Cairncross, B., Rubidge, B.S., Smith, R.M.H., Hancox, P.J., 2005. The Karoo basins of south-central Africa. Journal of African Earth Sciences 43, 211–253.

Cockburn, H.A.P., Brown, R.W., Summerfield, M., Seidl, M.A., 2000. Quantifying passive margin denudation and landscape development using a combined fission-track thermochronometry and cosmogenic isotope analysis approach. Earth and Planetary Science Letters 179, 429–435.

Corrigan, J.D., 1993. Apatite fission-track analysis of Oligocene strata in South Texas, USA; testing annealing models. Chemical Geology 104, 227–249.

Cornell, D.H., Thomas, R.J., Moen, H.F.G., Reid, D.L., Moore, J.M., Gibson, R.L., 2006. The Namaqua-Natal Province, in: Johnson, M.R., Anhaeusser, C.R., Tomas, R.J. (Eds.), The Geology of South Africa. Geological Society of South Africa. Johannesburg, Council for Geoscience, Pretoria, pp. 325–379.

de Wit, M.C.J., 1999. Post-Gondwana drainage and the development of diamond placers in Western South Africa. Economic Geology 94, 721–740.

de Wit, M.J., 2007. The Kalahari Epeirogeny and climate change: differentiating cause and effect from core to space. South African Journal of Geology 110, 367–392.

Dingle, R.V., Hendey, B.Q., 1984. Late Mesozoic and Tertiary sediment supply to the eastern cape basin (SE Atlantic) and paleo-drainage system in southwestern Africa. Marine Geology 56, 13–26.

Dingle, R.V., Robson, S.H., 1992. Southwestern Africa continental rise: structural and sedimentary evolution. In: Poag, C.W., Graciansky, P.C. (Eds.), Geologic Evolution of Atlantic Continental Rises. Van Nostrand Reinhold, New York, pp. 62–76.

Doucouré, C.A., de Wit, M.J., 2003. Old inherited origin for the present near bimodal topography of Africa. Journal of African Earth Sciences 36, 371–388.

Dumitru, T.A., 1995. A new computer automated microscope stage system for fission track analysis. Nuclear Tracks Radiation Measurements 21, 575–580.

Du Toit, A., 1926. Geology of South Africa. Oliver and Boyd Ltd, Edinburgh 449.

Eagles, G., 2007. New angles on South Atlantic opening. Geophysical Journal International 166, 353–361.

Eales, H.V., March, J.S., Cox, K.G., 1984. The Karoo igneous province: an introduction. In: Erlank, A.J. (Ed.), Petrogenesis of the Volcanic Rocks of the Karoo Province: Geological Society of South Africa Special Publication, 13, pp. 1–26.

Ebinger, C.J., Sleep, N.H., 1998. Cenozoic magmatism throughout east Africa resulting from impact of a single plume. Nature 395, 788–791.

Eglington, B.M., 2006. Evolution of the Namaqua–Natal Belt, southern Africa — a geochronological and isotope geochemical review. Journal of African Earth Sciences 46, 93–111.

Farley, K.A., 2000. Helium diffusion from apatite: general behavior as illustrated by Durango fluorapatite. Journal of Geophysical Research 105, 2903–2914.

Farley, K.A., 2002. (U–Th)/He dating: techniques, calibrations, and applications. Reviews in Mineralogy and Geochemistry 47, 819–844.

Farley, K.A., Wolf, R.A., Silver, L.T., 1996. The effects oflong alpha-stopping distance on (U-Th)/He ages. Geochimica et Cosmochimica Acta 60, 4223–4229.

Farley, K.A., Kohn, B.P., Pillans, B., 2002. The effects of secular disequilibrium on (U–Th)/He systematics and dating of Quaternary volcanic zircon and apatite. Earth and Planetary Science Letters 201, 117–125. http://dx.doi.org/10.1016/S0012-821X(02)00659-3.

Fleming, A., Summerfield, M.A., Stone, J.O.H., Fifield, L.K., Cresswell, R.G., 1999. Denudation rates for the southern Drakensberg escarpment, SE Africa, derived from in-situ-produced cosmogenic ^{36}Cl: initial results. Journal of the Geological Society of London 156, 209–212.

Flowers, R.M., Schoene, B., 2010. Mesozoic relief development and uplift of the eastern Kaapvaal craton, southern African Plateau from (U–Th)/He thermochronometry. Geology 38 (9), 827–830.

Flowers, R.M., Ketcham, R.A., Shuster, D.L., Farley, K.A., 2009. Apatite (U–Th)/He thermochronometry using a radiation damage accumulation and annealing model. Geochimica et Cosmochimica Acta 73, 2347–2365.

Frimmel, H.E., Frank, W., 1998. Neoproterozoic tectono-thermal evolution of the Gariep Belt and its basement, Namibia and South Africa. Precambrian Research 90, 1–28.

Fügenschuh, B., Schmid, S.M., 2003. Late stages of deformation and exhumation of an orogen constrained by fission track data: a case study in the Western Alps. Geological Society of America Bulletin 115, 1425–1440.

Galbraith, R.F., 1981. On statistical models for fission track counts. Mathematical Geology 13, 471–478.

Galbraith, R.F., 1990. The radial plot: graphical assessment of spread in ages. Nuclear Tracks and Radiation Measurements 17, 207–214.

Galbraith, R.F., Laslett, G.M., 1993. Statistical models for mixed fission-track ages. Nuclear Tracks and Radiation Measurements 21, 459–470.

Gallagher, K., Sambridge, M., 1994. Genetic algorithms: a powerful tool for large-scale nonlinear optimization problems. Computational Geosciences 20, 1229–1236.

Garver, J.I., Riley, B.C.D., Wang, G., 2002. Partial resetting of fission tracks in detrital zircon. Geotemas 4, 73–75.

Gerrard, I., Smith, G.C., 1983. Post-Paleozoic succession and structure of the southwestern African continental margin. In: Watkins, J.S., Drake, C.L. (Eds.), Studies in Continental Margin Geology: American Association of Petroleum Geologists, Memoir, 34, pp. 49–74.

Gleadow, A.J.W., Duddy, I.R., Green, P.F., Lovering, J.F., 1986. Confined fission track lengths in apatite: a diagnostic tool for thermal history analysis. Contributions to Mineralogy and Petrology 94, 405–415.

Gleadow, A.J.W., Duddy, I.R., 1981. A natural long-term annealing experiment for apatite. Nuclear Tracks 5, 169–174.

Green, P.F., Duddy, I.R., 1989. Some comments on paleotemperature estimation from apatite fission track analysis. Journal of Petroleum Geology 12, 111–114.

Gresse, P.G., von Veh, M.W., Frimmel, H.E., 2006. Namibian (Neoproterozoic) to Early Cambrian successions, in: Johnson, M.R., Anheausser, C.R., Thomas, R.J., (Eds.), The geology of South Africa. Geological Society of South Africa, Johannesburg, Council of Geoscience, Pretoria, pp. 395–420.

Grotzinger, J.P., Bowring, S.A., Saylor, B.Z., Kaufman, A.J., 1995. Biostratigraphic and geochronologic constraints on early animal evolution. Science 270, 598–604.

Gurnis, M., Mitrovica, J.X., Ritsema, J., van Heijst, H.-J., 2000. Constraining mantle density structure using geological evidence of surface uplift rates: the case of the African Superplume. Geochemistry, Geophysics, Geosystems 1 (11), 35. http://dx.doi.org/10.1029/1999GC000035.

Hawkesworth, C., Kelley, S., Turner, S., le Roex, A., Storey, B., 1999. Mantle processes during Gondwana break-up and dispersal. Journal of African Earth Sciences 28, 239–261.

Hourigan, J.K., Reiners, P.W., Brandon, M.T., 2005. U-Th zonation-dependent alpha-ejection in (U-Th)/He chronometry. Geochimica et Cosmochimica Acta 69, 3349–3365.

House, M.A., Wernicke, B.P., Farley, K.A., 1998. Dating topography of the Siera Nevada, California, using apatite (U–Th)/He ages. Nature 396, 66–69.

House, M.A., Wernicke, B.P., Farley, K.A., 2001. Paleo-geomorphology of the Sierra Nevada, California, from (U–Th)/He ages in apatite. American Journal of Science 301, 77–102.

Hurford, A.J., Green, P.F., 1983. The zeta age calibration of fission-track dating. Chemical Geology 41, 285–312.

Jelsma, H.A., de Wit, M.J., Thiart, C., Dirks, P.H.G.M., Viola, G., Basson, I.J., Anckar, E., 2004. Preferential distribution along transcontinental corridors of kimberlites and related rocks of southern Africa. South African Journal of Geology 107, 301–324.

Jelsma, H., Barnett, W., Richards, S., Lister, G., 2009. Tectonic settings of kimberlites. Lithos 1125, 155–165.

Johnson, M.R., van Vuuren, C.J., Visser, J.N.J., Cole, D.I., Wickens H.de V., Christie, A.D.M., Roberts, D.L., Brandl, G., 2006. Sedimentary rocks of the Karoo Supergroup, in: Johnson, M.R., Anheausser, C.R., Thomas, R.J., (Eds.), The geology of South Africa. Geological Society of South Africa, Johannesburg, Council of Geoscience, Pretoria, pp. 461–500.

Jourdan, F., Féraud, G., Bertrand, H., Watkeys, M.K., 2007. From flood basalts to the inception of oceanization: example from the ^{40}Ar/^{39}Ar high resolution picture of the Karoo large igneous province. Geochemistry, Geophysics, Geosystem 8, Q02002. http://dx.doi.org/10.1029/2006GC001392.

Kasuya, M., Naeser, C.W., 1988. The effect of α-damage of fission-track annealing in zircon. Nuclear Tracks and Radiation Measurements 14, 477–480.

Ketcham, R., Donelick, R., Donelick, M., 2000. AFTSolve: a program for multi-kinetic modeling of apatite fission-track data. Geological Materials Research 1, 1–32.

Ketcham, R., 2005. Forward and inverse modeling of low-temperature thermochronometry data. Reviews in Mineralogy and Geochemistry 58, 275–314.

Ketcham, R., Carter, A., Donelick, R.A., Barbarand, J., Hurford, A.J., 2007. Improved modeling of fission-track annealing in apatite. American Mineralogist 92, 799–810.

King, L.C., 1953. Cannons of landscape evolution. Geological Society of America Bulletin 64, 721–752.

Kounov, A., Niedermann, S., de Wit, M.J., Viola, G., Andreoli, M., Erzinger, J., 2007. Present denudation rates at selected sections of the South African escarpment and the elevated continental interior based on cosmogenic ^{3}He and ^{21}Ne. South African Journal of Geology 110, 235–248.

Kounov, A., Viola, G., de Wit, M.J., Andreoli, M., 2008. A Mid Cretaceous paleo-Karoo River valley across the Knersvlakte plain (northwestern coast of South Africa): evidence from apatite fission-track analysis. South African Journal of Geology 111, 409–420.

Kounov, A., Viola, G., de Wit, M.J., Andreoli, M.A.G., 2009. Denudation along the Atlantic passive margin: new insights from apatite fission-track analysis on the western coast of South Africa. In: Lisker, F., Ventura, B., Glasmacher, U. (Eds.), Geological Society, London, Special Publications, 324, pp. 287–306.

Laslett, G.M., Green, P.F., Duddy, I.R., Gleadow, A.J.W., 1987. Thermal annealing of fission tracks in apatite 2. A quantitative analysis. Chemical Geology (Isotope Geoscience Section) 65, 1–13.

Lithgow-Bertelloni, C., Silver, P., 1998. Dynamic topography, plate driving forces and the African superswell. Nature 395, 269–272.

Meesters, A.G.C.A., Dunai, T.J., 2002. Solving the production–diffusion equation for finite diffusion domains of various shapes; part II, application to cases with alpha-ejection and nonhomogeneous distribution of the source. Chemical Geology 186, 57–73.

Moore, A.E., 1999. A reappraisal of epeirogenic flexure axes in southern Africa. South African Journal of Geology 102, 363–376.

Moore, A.E., Blenkinsop, T.G., Cotterill, F.P.D., 2008. Controls of post-Gondwana alkaline volcanism in southern Africa. Earth and Planetary Science Letters 268, 151–164.

Moore, A.E., Blenkinsop, T.G., Cotterill, F., 2009. Southern African topography and erosion history: plumes or plate tectonics? Terra Nova 21, 310–315.

Mvondo, F., Dauteuil, O., Guillocheau, F., 2011. The Fish River canyon (Southern Namibia): a record of Cenozoic mantle dynamics? Comptes Rendus Geoscience 343, 478–485.

Nürnberg, D., Müller, R.D., 1991. The tectonic evolution of the South Atlantic from late Jurassic to present. Tectonophysics 191, 27–53.

Nyblade, A., Robinson, S., 1994. The African superswell. Geophysical Research Letters 21, 765–768.

Partridge, T.C., 1998. Of diamonds, dinosaurs and diastrophism: 150 million years of landscape evolution in southern Africa. South African Journal of Geology 101, 167–185.

Partridge, T.C., Maud, R.R., 1987. Geomorphic evolution of southern Africa since the Mesozoic. South African Journal of Geology 90, 179–208.

Philips, D., Kiviets, G.B., Biddulph, M.G., Madav, M.K., 2000. Cenozoic volcanism. In: Partridge, T.C., Maud, R.R. (Eds.), The Cenozoic of Southern Africa. Oxford University Press, Oxford, UK, pp. 182–197.

Raab, M.J., Brown, R.W., Gallagher, K., Carter, A., Weber, K., 2002. Late Cretaceous reactivation of major crustal shear zones in northern Namibia: constraints from apatite fission track analysis. Tectonophysics 349, 75–92.

Rabinovich, P.D., LaBrecque, J., 1979. The Mesozoic South Atlantic Ocean and evolution of its continental margin. Journal of Geophysical Research 84, 5973–6002.

Rahn, M.K., Brandon, M.T., Batt, G.E., Garver, J.I., 2002. A zero-damage model for fission-track annealing in zircon. American Mineralogist 89, 473–484.

Reid, D.L., Rex, D.C., 1994. Cretaceous dikes associated with the opening of the South Atlantic: the Mehlberg dike, northern Richtersveld. South African Journal of Geology 97, 135–145.

Reiners, P.W., 2005. Zircon (U–Th)/He thermochronometry. Reviews in Mineralogy and Geochemistry 58, 151–179.

Reiners, P.W., Ehlers, T.A., Garver, J.I., Gran-Mitchell, S., Montgomery, D., Vance, J.A., Nicolescu, S., 2002. Late Miocene exhumation and uplift of the Washington Cascades. Geology 30, 767–770.

Reiners, P.W., Zhou, Z., Ehlers, T.A., Xu, C., Brandon, M.T., Donelick, R.A., Nicolescu, S., 2003. Post-orogenic evolution of the Dabie Shan, eastern China, from (U–Th)/He and fission-track thermochronology. American Journal of Science 303, 489–518.

Reiners, P.W., Spell, T.L., Nicolescu, S., Zanetti, K.A., 2004. Zircon (U–Th)/He thermo chronometry: He diffusion and comparisons with $^{40}Ar/^{39}Ar$ dating. Geochimica et Cosmochimica Acta 68, 1857–1887. http://dx.doi.org/10.1016/j.gca. 2003.10.021.

Roberts, G.G., White, N., 2010. Estimating uplift rate histories from river profiles using African examples. Journal of Geophysical Research 115, B02406. http://dx.doi.org/10.1029/2009JB006692.

Rust, D.J., Summerfield, M.A., 1990. Isopach and borehole data as indicators of rifted margin evolution in southwestern Africa. Marine and Petroleum Geology 7, 277–287.

Simpson, G.D.H., 2004. Dynamic interactions between erosion, deposition and three-dimensional deformation in compressional fold belt settings. Journal of Geophysical Research 109, F03007. http://dx.doi.org/10.1029/2003JF000111.

Shuster, D.L., Flowers, R.M., Farley, K.A., 2006. The influence of natural radiation damage on helium diffusion kinetics in apatite. Earth and Planetary Science Letters 249, 148–161.

Skinner, E.M.W., Truswell, J.F., 2006. Kimberlites, in: Johnson, M.R., Anheausser, C.R., Thomas, R.J., (Eds.), The geology of South Africa. Geological Society of South Africa, Johannesburg, Council of Geoscience, Pretoria, pp. 651–659.

Smith, C.B., Allsopp, H.L., Kramers, J.D., Hutchinson, G., Roderick, J.C., 1985. Emplacement ages of Jurassic–Cretaceous South African kimberlites by the Rb–Sr method on phlogopite and whole rock samples. Transactions of the Geological Society of South Africa 88, 249–266.

Stüwe, K., White, L., Brown, R., 1994. The influence of eroding topography on steady-state isotherms. Application to fission track analysis. Earth and Planetary Science Letters 124, 63–74.

Tagami, T., 2005. Zircon fission-track thermochronology and applications to fault studies. Reviews in Mineralogy and Geochemistry 58, 95–122.

Tagami, T., Dumitru, T.A., 1996. Provenance and history of the Franciscan accretionary complex: constraints from zircon fission track thermochronology. Journal of Geophysical Research 101, 11353–11364.

Tagami, T., Galbraith, R.F., Yamada, R., Laslett, G.M., 1998. Revised annealing kinetics of fission tracks in zircon and geological implications. In: Van den Haute, P., de Corte, F. (Eds.), Advances in Fission-track Geochronology. Kluwer Academic Publishers, Dordrecht, pp. 99–114.

Tankard, A., Welsink, H., Aukes, P., Newton, R., Stettler, E., 2009. Tectonic evolution of the Cape and Karoo basins of South Africa. Marine and Petroleum Geology 26, 1379–1412. http://dx.doi.org/10.1016/j.marpetgeo.2009.01.022.

Tinker, J., de Wit, M., Brown, R., 2008. Mesozoic exhumation of the southern Cape, South Africa, quantified using apatite fission track thermochronology. Tectonophysics 1–4, 77–93.

Thamm, A.G., Johnson, M.R., 2006. The Cape Supergroup, In: Johnson, M.R., Anheausser, C.R., Thomas, R.J., (Eds.), The geology of South Africa. Geological Society of South Africa, Johannesburg, Council of Geoscience, Pretoria, pp. 443–460.

Trumbull, R.B., Reid, D.L., de Beer, C., van Acken, D., Romer, R.L., 2007. Magmatism and continental breakup at the west margin of southern Africa: a geochemical comparison of dolerite dikes from northwestern Namibia and the Western Cape. South African Journal of Geology 110, 477–502.

Veevers, J.J., Cole, D.I., Cowan, E.J., 1994. Southern Africa: Karoo Basin and Cape Fold Belt. In: Veevers, J.J., Powell, C.M.A. (Eds.), Permian-Triassic pangean basins and foldbelts along the panthalassan margin of Gondwanaland: Geological Society of America, Memoirs, 184, pp. 223–280.

Viola, G., Andreoli, M., Ben Avraham, Z., Stengel, I., Reshef, M., 2005. Offshore mud volcanoes and onland faulting in southwestern Africa: Neotectonic implications and constraints on the regional stress field. Earth and Planetary Science Letters 231, 147–160.

Viola, G., Anczkiewicz, R., 2008. Exhumation history of the Red River shear zone in northern Vietnam: new insights from zircon and apatite fission-track analysis. Journal of Asian Earth Sciences 33, 78–90.

Viola, G., Kounov, A., Andreoli, M.A., Mattila, J., 2012. Brittle tectonic evolution along the western margin of South Africa: more than 500 Myr of continued reactivation. Tectonophysics 514–517, 93–114. http://dx.doi.org/10.1016/j.tecto.2011.10.009.

Visser, J.N.J., 1990. The age of the late Palaeozoic glaciogene deposits in southern Africa. South African Journal of Geology 93, 366–375.

Wolf, R.A., Farley, K.A., Kass, D.M., 1998. Modeling of the temperature sensitivity of the apatite (U–Th)/He thermochronometer. Chemical Geology 148, 105–114.

Yamada, R., Tagami, T., Nishimura, S., Ito, H., 1995. Annealing kinetics of fission tracks in zircon: an experimental study. Chemical Geology 122, 249–258.

Zeilinger, G., Schlunegger, F., Simpson, G., 2005. The Oxaya anticline (northern Chile): a buckle enhanced by river incision? Terra Nova 17, 368–375.